European Journal of Nuclear Medicine and Molecular Imaging (2025) 52:4639–4651
https://doi.org/10.1007/s00259-025-07379-9

ORIGINAL ARTICLE

Glucose metabolism in hyper-connected regions predicts neurodegeneration and speed of conversion in Alzheimer's disease

Alice Galli[1,2] · Marianna Inglese[3] · Luca Presotto[4] · Rachele Malito[5] · Xin Di[6] · Nicola Toschi[3] · Andrea Pilotto[1,2] · Alessandro Padovani[1,2] · Cristina Tassorelli[5,7] · Daniela Perani[8] · Arianna Sala[10,11,12] · Silvia Paola Caminiti[7,9]

Received: 19 February 2025 / Accepted: 21 May 2025 / Published online: 5 June 2025

Abstract

Purpose Here, we combined a longitudinal design to assess whole-brain hyper- and hypo-connectivity in the different clinical phases of Alzheimer's disease (AD) with a multimodal approach to understand how such connectivity changes were related to glucose hypometabolism.

Methods We selected a longitudinal cohort of $N = 66$ subjects with clinical, cerebrospinal fluid and FDG-PET assessments, from Alzheimer's Disease Neuroimaging Initiative (ADNI) database. $N = 31$ AD individuals were assessed at three stages: mild cognitive impairment (AD-MCI, T0), early phase of dementia (mild-AD, T1) and dementia (AD-D, T2). We included $N = 35$ age/sex-matched healthy controls. We assessed longitudinal metabolic connectivity using Pearson's correlation, clustering analysis and graph theory metrics.

Results In the MCI-AD stages, hypo- and hyper-connectivity coexisted. Data-driven, longitudinal clustering analysis identified specific pathological clusters: a default mode network cluster, with prevalent hypo-connectivity and severe, persistent hypometabolism; a limbic cluster showing hyper-connectivity and steeper metabolic decline. Metabolism in hyper-connected limbic regions showed a mediation effect on worsening of AD-like parieto-temporal hypometabolism and predicted faster conversion to dementia.

Conclusion Hypo- and hyper-connectivity, especially in early stages, may have different roles in AD neurodegenerative processes, with metabolism in hyper-connected regions acting as a mediator on the neurodegeneration of core regions of AD pathology.

Keywords Glucose metabolism · Prodromal · Mild cognitive impairment · Hyper-connectivity · Hypo-connectivity · Graph theory

Arianna Sala and Silvia Paola Caminiti joint senior authors.

✉ Silvia Paola Caminiti
silviapaola.caminiti@unipv.it

1 Neurology Unit, Department of clinical and experimental sciences, University of Brescia, Brescia 25123, Italy

2 Laboratory of Digital Neurology and Biosensors, University of Brescia, Brescia 25123, Italy

3 Department of Biomedicine and Prevention, University of Rome Tor Vergata, Rome 0133, Italy

4 Università degli Studi Milano-Bicocca, Milan 20126, Italy

5 IRCCS Mondino Foundation, 27100 Pavia, Italy

6 Department of Biomedical Engineering, New Jersey Institute of Technology, Newark, NJ 07102, USA

7 Department of Brain and Behavioral Sciences, University of Pavia, 27100 Pavia, Italy

8 IRCCS San Raffaele Scientific Institute, Milan 20132, Italy

9 University of Pavia, Viale Golgi 19, 27100 Pavia, Italy

10 Coma Science Group, GIGA Consciousness, GIGA Institute, University of Liège, Liège, Belgium

11 NeuroRecovery Lab, GIGA Consciousness, GIGA Institute, University of Liège, Liège, Belgium

12 NeuroRehab & Consciousness Clinic, Neurology Department, University Hospital of Liège, Liège, Belgium

Introduction

Alzheimer's disease (AD) is biologically characterized by pathological accumulations of amyloid beta (Aβ) plaques and neurofibrillary tau tangles in the brain [1]. In AD, Aβ and tau pathology, primarily accumulating in the default-mode network (DMN) and limbic network, largely spread through interconnected regions [2–4], making brain connectivity a valuable tool to understand the pathophysiology of AD. Furthermore, previous works have used brain connectivity alterations to predict early AD-related cognitive decline, even in cognitively healthy elderly people showing subtle Aβ and tau accumulation [5]).

Previous studies largely focused on investigating the association between pathology and hypo-connectivity [6, 7]. Together, patterns of increased functional connectivity, i.e. hyper-connectivity, have been reported in the prodromal mild cognitive impairment (MCI) phase and AD dementia, particularly involving the local connectivity within the limbic network, including the medial temporal lobe [8–12]. As for the latter, some authors proposed a mechanism where the disconnection between the limbic network and posterior DMN would lead to hyper-connectivity within the same limbic network [13]. Others have suggested Aβ pathology to be at the basis of the observed limbic hyper-connectivity [7]. Recently, a large longitudinal study showed that anterior-temporal (AT) hyper-connectivity is specifically associated with Alzheimer's pathology, predicting faster glucose hypometabolism and dementia onset. This hyper-connectivity correlates with Aβ burden and reduced cognitive performance and mediates speed of disease progression [14]. Another recent study, by Roemer-Cassiano and colleagues, showed that temporal hyper-connectivity mediates the effect of Aβ burden on faster tau accumulation [7]. These findings suggest that hyper-connectivity is not compensatory but may actively drive pathology and neurodegeneration [7, 14]. The detected hyper-connectivity could be a sign of high processing burden and noisy inefficient synaptic communication [15].

The mechanisms underlying hyper-connectivity in AD, however, remain partially unclear [16].

The majority of studies assessing connectivity in AD have adopted either unimodal cross-sectional [11] or longitudinal [12, 17] or multimodal cross-sectional [18, 19] designs.

Multimodal longitudinal investigations assessing the crosstalk between time-dependent metabolic connectivity reconfigurations and local brain hypometabolism in highly homogeneous groups of patients with assessed evolution in clinical and biomarker profiles may provide enhanced insights about neurodegenerative mechanisms. Here, we combined a longitudinal design to assess whole-brain hyper- and hypo-connectivity in the different clinical phases of the same AD cohort with a longitudinal multimodal approach to understand how such connectivity changes can be related to glucose hypometabolism. In detail, we used 2-[18 F] fluoro-2-deoxy-D-glucose (FDG)-positron emission tomography (PET) estimation to characterize glucose metabolism and brain metabolic connectivity changes [20] in the very same cohort of subjects with clinical and cerebrospinal fluid biomarkers profiles, followed up longitudinally from MCI to full-blown AD dementia. To this end, we analyzed a group of amnestic MCI subjects from the Alzheimer's Disease Neuroimaging Initiative (ADNI) database, positive for AD pathology and with available clinical and neuroimaging (FDG-PET and magnetic resonance imaging (MRI)) follow-up data at three clinical phases, namely: (i) MCI due to AD (AD-MCI), T0 baseline; (ii) early phase of AD dementia (mild-AD), T1; (iii) full-blown AD dementia (AD-D), T2. We assessed connectivity rearrangements in terms of hypo-, hyper-connectivity and graph theory metrics, in the patients compared to a healthy control (HC) group. By implementing a clustering process on the measures of hypo- and hyper-connectivity, we defined both the connectivity features specific to various stages and those present constantly over time.

Materials and methods

Participants

We retrospectively included amnestic MCI subjects from ADNI1, ADNI2, ADNI3, and ADNI-GO (details: *ADNI website*). ADNI's amnestic MCI criteria required memory decline (CDR = 0.5), MMSE 24–30, no dementia, and no severe psychiatric comorbidities. Clinical progression to dementia was defined by a CDR global score ≥1 and an MMSE score <24 [21].

We selected amyloid, tau and neurodegeneration-positive (A + T + N+) MCI cases diagnosed as AD-MCI per NIA-AA classification system [1]. Amyloid positivity (A+) was determined by CSF Aβ−42 levels below 192 pg/mL, with the exception of two cases where CSF assessments were not available. As in our MCI cases with both CSF and amyloid-PET data (n = 15), there was 100% agreement between the two markers, for the two additional cases where only CSF results were not available, positivity at amyloid-PET alone was used to determine the A+ status.

Phosphorylated-Tau positivity (T+) was defined by CSF p-Tau (> 27 pg/mL). Neurodegeneration (N+) was confirmed via FDG-PET, analyzed on a SPM-based procedure, and evaluated for the presence of the typical AD pattern

involving the temporo-parietal regions, precuneus and posterior cingulate cortex (*See FDG-PET procedures*).

We included MCI subjects with clinical, T1-MRI, and FDG-PET assessments at three stages: T0 (AD-MCI), T1 (mild-AD, dementia conversion, mean follow-up 2.02 ± 1.18 years), and T2 (AD-D, ≥2 years post-conversion, mean follow-up 4.36 ± 2.02 years). T2 was chosen to assess advanced-stage connectivity changes. ADNI Memory Score (ADNI-Mem) was obtained at all stages [17].

We included a group of healthy controls (HC) starting from a previously validated group [18] and used for subsequent comparisons. We selected only subjects who: (1) had no evidence of cognitive impairment at baseline and were cognitively stable at an average 4-year follow-up [18]; (2) were A-T-N-, according to the same criteria described above; (3) were age- and sex- matched to the AD-MCI group; (4) had T1-MRI, FDG-PET, and clinical assessments available at the same three time points as the AD group (i.e., mean follow-up times at T1: 1.93 ± 0.78 years and T2: 3.96 ± 1.89 years, respectively). Of note, the latter inclusion criteria, i.e. availability of imaging and clinical data at the same three clinical stages as the patients, was introduced to isolate pathological changes going beyond those attributable to normal aging. The final sample comprised $n = 31$ AD-MCI and $n = 35$ HC subjects. See Table 1.

In our sample, APOE ε4 allele frequencies were as follows: among HC, ε2/ε4 = 3%, ε3/ε4 = 14%, and ε4/ε4 = 3%, resulting in an overall ε4 carrier rate of 20%; in contrast, AD patients showed ε3/ε4 = 55% and ε4/ε4 = 16%, with no ε2/ε4 cases, yielding a total ε4 carrier rate of 71%.

FDG-PET procedures

ADNI acquisition procedures are detailed in the "ADNI PET technical procedures manual, version 9.5" (https://adni.loni.usc.edu/methods/pet-analysis-method/pet-analysis/). We combined the last three 5-min FDG-PET frames into a single 15-min static image for consistency [18]. Images underwent visual quality checks and were pre-processed using SPM12 (https://www.fil.ion.ucl.ac.uk/spm/) [22, 23]. FDG-PET images were normalized to a dementia-specific MNI template [22] and smoothed with a Gaussian Kernel of 8 mm FWHM. We applied global mean scaling to each spatially normalized and smoothed FDG-PET image (FDG-PET SUVr) in order to account for between-subject uptake variability [24]. Then, FDG-PET SUVr images were analyzed using a validated single-subject SPM-based procedure [25], which generated individual SPM-t maps [18]. These maps quantified the severity of hypometabolism, with t-scores >1.7, $p < 0.05$ indicating regional hypometabolism compared to HC distribution. A nuclear medicine expert, blinded to clinical data, reviewed these t-maps for the presence of hypometabolism in the precuneus, posterior cingulate, and temporo-parietal regions. The FDG-PET AD pattern positivity further supported the AD-like diagnosis in our cohort.

MRI procedures

We included structural 3D MRIs (1.5 or 3 Tesla T1-weighted Magnetization Prepared Rapid Acquisition with Gradient Echo (MPRAGE) or Inversion Recovery Fast Spoiled Gradient Recalled (IR-FSPGR)) from Siemens, Philips, and GE scanners. For further details on MRI acquisition procedure: https://adni.loni.usc.edu/methods/mri-tool/mri-acquisition/.

Network construction

We segmented the structural MRI images to create probability maps for grey matter (GM) using SPM unified segmentation function. GM masks were thresholded and binarized at a threshold of 0.3 in order to exclude spurious voxels [26].

Table 1 Baseline characteristics of the subjects included

	HC ($N = 35$)	MCI-due to AD ($N = 31$)	p-value
Age	71.49 ± 3.28	72.38 ± 8.21	0.753
Sex (M: F)	17:18	18:13	0.441
Education	16.69 ± 2.69	16.03 ± 3.15	0.473
CSF Aβ−42	1602.12 ± 594.26	151.67 ± 33.19	**< 0.001**
CSF p-tau	19.35 ± 5.97	185.25 ± 51.24	**< 0.001**
APOE ε4 carrier	7 (20%)	22 (71%)	**< 0.001**
MMSE T0 AD-MCI	29.03 ± 1.32	26.61 ± 2.04	**< 0.001**
MMSE T1 mild-AD	29.17 ± 1.15	23.23 ± 4.00	**< 0.001**
MMSE T2 AD-D	29.18 ± 1.14	19.23 ± 6.57	**< 0.001**
ADNI-Mem T0 AD-MCI	1.07 ± 0.45	−0.19 ± 0.30	**< 0.001**
ADNI-Mem T1 mild-AD	1.14 ± 0.45	−0.64 ± 0.41	**< 0.001**
ADNI-Mem T2 AD-D	1.14 ± 0.45	−1.11 ± 0.65	**< 0.001**

Data reported as mean ± standard deviation. Abbreviations: *HC* Healthy Controls, *MCI* Mild Cognitive Impairment, *APOE* Apolipoprotein-E, *MMSE* Mini Mental State Examination, *ADNI-Mem* Alzheimer's Disease Neuroimaging Initiative Memory Score, *CSF* Cerebrospinal Fluid, Aβ−42, amyloid-β 42; p-tau, phosphorylated tau

The automated Anatomical Labelling Atlas (116 AAL) and FDG-PET SUVr images were transformed into each MRI individual's native space by means of spatial normalization to the inverse transformation matrix [27]. Finally, we extracted the FDG-PET SUVr from 116 AAL regions (i.e., network nodes) within the obtained AAL atlas intersected with individual GM mask.

Statistical analysis

We compared demographics, clinical and biological CSF and PET features of the included sample between patients and controls using Mann Whitney's U-test or Chi-squared test. We assessed the longitudinal rate of change in ADNI-Mem scores using a linear mixed-effects (LME) model. This analysis included both between-group comparisons (patients vs. controls) over time, as well as within-group comparisons across different stages (T1 mild-AD and T2 AD-D) against T0 AD-MCI. The LME model was adjusted for age, sex, and education level, and accounted for the repeated measurements of ADNI-Mem scores for each subject. To appropriately account for the structure of the longitudinal data, we specified a random intercept for each participant to capture inter-individual variability in ADNI-Mem scores. Additionally, to account for potential individual differences in the rate of cognitive decline, we included a random slope for the time variable, allowing us to model subject-specific trajectories of change over time. The LME approach was chosen for its ability to handle correlated data points within the same individual, even in the presence of missing data, unequally spaced observations, or unbalanced group samples [28].

All statistical analyses were performed with SPSS version 26.

Brain hypometabolism features

We performed a voxel-wise group analysis on SPM to extract regional hypometabolism characterizing AD individuals at each stage (T0 AD-MCI, T1 mild-AD, T2 AD-D) as compared to the HC group, considering age as a covariate of non-interest. We set a whole-brain Family Wise Error (FWE) corrected cluster-level significance threshold of $p = 0.05$, with an initial voxel-level threshold of $p < 0.001$ uncorrected. Only clusters larger than 100 voxels were deemed to be significant.

Metabolic connectivity analysis

We assessed molecular connectivity between brain regions using Pearson's correlation analysis. We computed a correlation matrix at each stage employing MATLAB's correlation function. Correlation matrix provides an estimation of the strength of connectivity between networks' nodes. To ensure a fair comparison, we assessed significant differences between each clinical group and a subgroup of HC matched for sample size, age, and sex. Following [29], we applied Fisher's r-to-z transformation to each Pearson correlation coefficient. This transformation converts correlation coefficients into a normally distributed variable while preserving the original sign of the correlation, enabling direct statistical comparisons. The resulting z-scores were used for statistical comparisons. We performed a z-test, and we applied a $p < 0.05$ threshold with False Discovery Rate (FDR) correction to the z-scores matrices to identify significantly altered connections in patients compared to HC.

The number of altered connections, identified by significant z-scores, was normalized by dividing by the total number of possible connections, calculated as $n\,(n-1)$, where n represents the number of nodes ($n = 116$).

The z-score entries can be negative or positive, indicating hypo-connectivity or hyper-connectivity, respectively.

Clustering analysis

The following indexes were computed for each node to represent comprehensively the changes in connection pattern:

- MeanAbsoluteZ: the mean of all the absolute values of all z-scores (excluding zero values), with higher values indicating greater network alterations;
- MeanPositiveZ: the mean of all positive z-scores (excluding zero values), with higher values indicating greater hyper-connectivity in patients than controls;
- MeanNegativeZ: the mean of all negative z-scores (excluding zero values), with higher values indicating greater hypo-connectivity in patients than controls;
- MeanAllZ: the mean of all z-scores (positive or negative) indicates the average amount of hypo- (negative sign) and hyper-connectivity (positive sign).

We analyzed connectivity shifts using KMeans clustering (scikit-learn, 2024) with Euclidean distance. The optimal cluster number (k) was determined via the elbow method (k = 2–8) [30].

We used two separate clustering algorithms:

1) Single Time Frame Clustering (STFC) to analyze "stage-specific connectivity" changes. Connectivity changes, represented as MeanAbsoluteZ values, were independently clustered at three different stages. For each group and time point (T0 AD-MCI, T1 mild-AD, T2 AD-D), the clustering algorithm processed an array of $(n \times 1)$ scores, where $n = 116$ corresponds to the number of brain regions;

2) Longitudinal Clustering (LC) to monitor the "evolution of connectivity" patterns over the course of AD within the same cohort of patients ($t = 3$: T0 AD-MCI, T1 mild-AD, T2 AD-D). The clustering algorithm received an input array of ($n \times t$) × z-scores, formed by concatenating the entire set of four MeanZ values across the three time-points. Brain regions that consistently clustered together across all examined time-points in the LC analysis were identified as cluster-specific nodes.

Then, we used repeated-measure ANOVA ($p < 0.05$, Bonferroni) to compare the mean metabolism SUVr values, from LC-derived clusters over time (i.e. using the mean SUVr values at T0 AD-MCI, T1 mild-AD, T2 AD-D as variables of interest). We conducted a mediation analysis to test whether the relationship between the mean metabolism within parieto-temporal AD-like regions at T0 and T2 was mediated via baseline metabolism within LC-derived clusters. Parieto-temporal AD-like regions included precuneus, posterior cingulate cortex, inferior parietal lobule, angular gyri and middle temporal gyri based on [31]. Linear regression (adjusted β, p-values) was computed for each path of the model [32]. The significance of the indirect effect was determined using Sobel's test.

A further linear regression model was used to test the association between metabolism within LC-derived clusters and the time of clinical conversion to dementia, adjusting for age, sex and education.

Similarity between clusters derived from LC procedure and functional network atlases [33] was computed using Network Correspondence Toolbox developed in Python (cbig_network_correspondence on Google Collaboratory, 2024). We implemented a spin test to assess the spatial overlap between each cluster and the functional network atlas (1.000 permutations).

Graph theory metrics

To examine differences in network architecture between AD and HC groups across stages (T0 AD-MCI, T1 mild-AD, and T2 AD-D), we analyzed specific metrics, using the BRAPH software (Brain Analysis using Graph Theory ([34] http://braph.org) (Supplementary Material 2).

Results

Longitudinal evolution of cognitive impairment and brain metabolism

The estimated rate of change in ADNI-Mem scores indicated a significant cognitive decline in the AD group ($N = 31$) compared to the HC group ($N = 35$) (estimate [SE]: 1.36 [0.1]; $p < 0.001$). Compared to T0, only the AD group demonstrated a significant reduction in ADNI-Mem scores (estimate at T1 mild-AD [SE]: −0.45 [0.08]; $p < 0.001$; estimate at T2 AD-D [SE]: −0.92 [0.1]; $p < 0.001$) (Table 1).

The AD-like hypometabolism pattern, primarily involving the temporo-parietal cortex, was already fully expressed and detectable in the AD-MCI stage and maintained – but worsening - along the disease course (Supplementary Fig. 1).

Metabolic connectivity results

During the AD-MCI stage, subjects showed significant differences in connectivity compared to age- and sex-matched HC ($p < 0.05$ FDR-corrected). Specifically, 4% of the total functional connections showed significant alterations in connectivity, comprising both hypo- and hyper-connectivity. Hypo-connectivity was widely distributed across frontal regions (medial and orbital frontal cortices, rectus gyrus, superior frontal gyrus), occipital areas (superior, middle, and inferior occipital gyri, cuneus, lingual gyrus), parietal regions (supramarginal gyrus, angular gyrus, superior and inferior parietal lobules), temporal areas (middle and inferior temporal gyri, temporal poles), cerebellar regions, and subcortical structures including the caudate nucleus, putamen, and thalamus. Hyper-connectivity was predominantly observed between the vermis, frontal regions (medial and orbital frontal cortices, rectus gyrus, superior frontal gyrus, rolandic operculum), superior temporal gyrus, inferior occipital gyrus, and the olfactory cortex.

In the mild-AD stage, 2% of connections were altered, exclusively characterized by hypo-connectivity, involving frontal regions (precentral, superior, middle, inferior, and medial orbital frontal cortices, rectus gyrus, opercular and triangular parts of the inferior frontal gyrus), occipital areas (superior, middle, and inferior occipital gyri, cuneus, lingual and fusiform gyri), parietal regions (supramarginal gyrus, angular gyrus, superior and inferior parietal lobules, precuneus), temporal areas (middle and inferior temporal gyri, temporal poles), as well as subcortical structures including the thalamus, putamen, pallidum, and caudate nucleus.

In the AD-D stage, 3% of connections were characterized by both hypo- and hyper-connectivity, involving widespread hypo-connectivity of frontal regions, insular cortex, and cingulate cortex (anterior, middle, posterior), with occipital areas, parietal regions, temporal regions, subcortical structures and cerebellar regions. Hyper-connectivity was found between vermis and the supplementary motor areas, postcentral gyrus, paracentral lobule, medial and orbital frontal cortices, insula, olfactory cortex, parahippocampal gyrus, hippocampus, and amygdala, as well as increased coupling between cerebellar lobules and thalamic structures (Fig. 1).

Hypo-connectivity was mostly driven by negative correlations in patients but positive in controls (-/+), and hyper-connectivity was mostly due to positive correlations in patients but negative in controls (+/-) (Supplementary Material 4 and Supplementary Fig. 2).

Clustering analysis

STFC identified two clusters per stage that fairly corresponded to "altered" or "unaffected" regions.

The regions consistently altered from MCI to AD dementia stages included the frontal cortex (superior, middle, medial, orbital, inferior frontal areas, and rectus), occipital cortex (superior, middle, inferior occipital gyri, and cuneus), parietal cortex (superior, inferior parietal lobules, supramarginal, angular gyri, and precuneus), and temporal cortex (middle and inferior temporal gyri), along with the posterior cingulate cortex and vermis (Fig. 2a).

LC revealed three distinct clusters, each showing unique patterns of connectivity changes over the three stages. *Cluster* 0, representing with low-intensity connectivity changes regions, included the middle cingulate cortex, Heschl gyrus, temporal pole, and cerebellar cortex. *Cluster 1* consisted of nodes showing highest hypo-connectivity, in the precuneus, superior and inferior parietal lobule, middle temporal lobe, occipital cortex, and ventromedial frontal cortex. *Cluster 2* encompassed regions with greatest hyper-connectivity, namely, the hippocampus, amygdala and vermis (Fig. 2b).

In the spatial overlap analysis, Cluster 1 showed the greater significant overlap with DMN (DICE score = 0.38, $p = 0.006$); Cluster 2 showed the greatest overlap, with a still not-significant trend, with the Limbic Network (DICE score = 0.13, $p = 0.103$) (Fig. 3).

Upon analyzing the average metabolic profiles of each cluster obtained from the LC, a distinct pattern became apparent. Compared to HC, metabolism within each cluster was significantly lower in patients, at each stage ($p < 0.001$). Compared to Cluster 0, among patients, only Cluster 1 showed significant hypometabolism, ($p < 0.001$), at all stages (Fig. 2c).

Notably, only Cluster 2 showed a significant SUVr decrease over time, with the AD-D stage showing greater hypometabolism than AD-MCI ($p = 0.033$).

In the mediation analysis, we first tested the direct effect of metabolism within the parieto-temporal AD-like regions at T0 (AD-MCI) and T2 (AD-D), which was positive and significant (β = 0.498, $p = 0.025$). Second, we found a significant indirect effect between the independent variable, namely the metabolism within AD-like regions at T0 (AD-MCI), and metabolism within Cluster 1 (β = 0.449, $p = 0.011$), and Cluster 2 (β = 0.866, $p < 0.001$). Third, we showed that only metabolism within Cluster 2 at T0 significantly predicted metabolism within AD-like regions at T2 (β = 0.439, $p = 0.036$) (Fig. 4). The significance of the effect was confirmed using Sobel's test (Sobel's Test statistic = 2.26, $p = 0.024$).

Finally, the linear regression model showed a significant and positive association between metabolism within Cluster 2 at T0 and the time of clinical conversion to dementia (β = 0.442, $p = 0.022$) - adjusting for age, sex, and education.

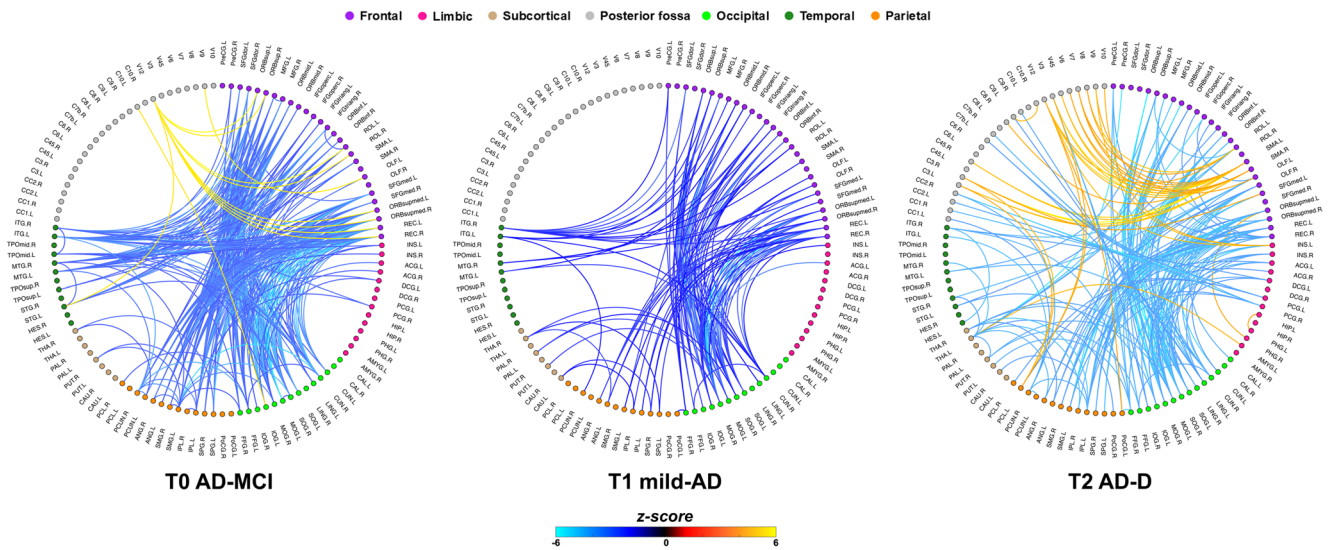

Fig. 1 Metabolic connectivity analyses. Network plots illustrating significant metabolic connectivity alterations in patients compared to controls at each disease stage ($p < 0.05$, FDR-corrected). Circles represent different macro-areas: purple = Frontal, pink = Limbic, mustard = Subcortical, grey = Posterior Fossa, green = Occipital, dark green = Temporal, orange = Parietal. The color gradient reflects the strength and direction of connectivity changes, with light blue to blue lines indicating hypo-connectivity, while red-to-yellow lines indicate hyper-connectivity. Network visualization was performed using the *ggraph* R package. Abeviations: AD, Alzheimer's Disease; MCI, Mild Cognitive Impairment; AD-D, Dementia due to Alzheimer's Disease

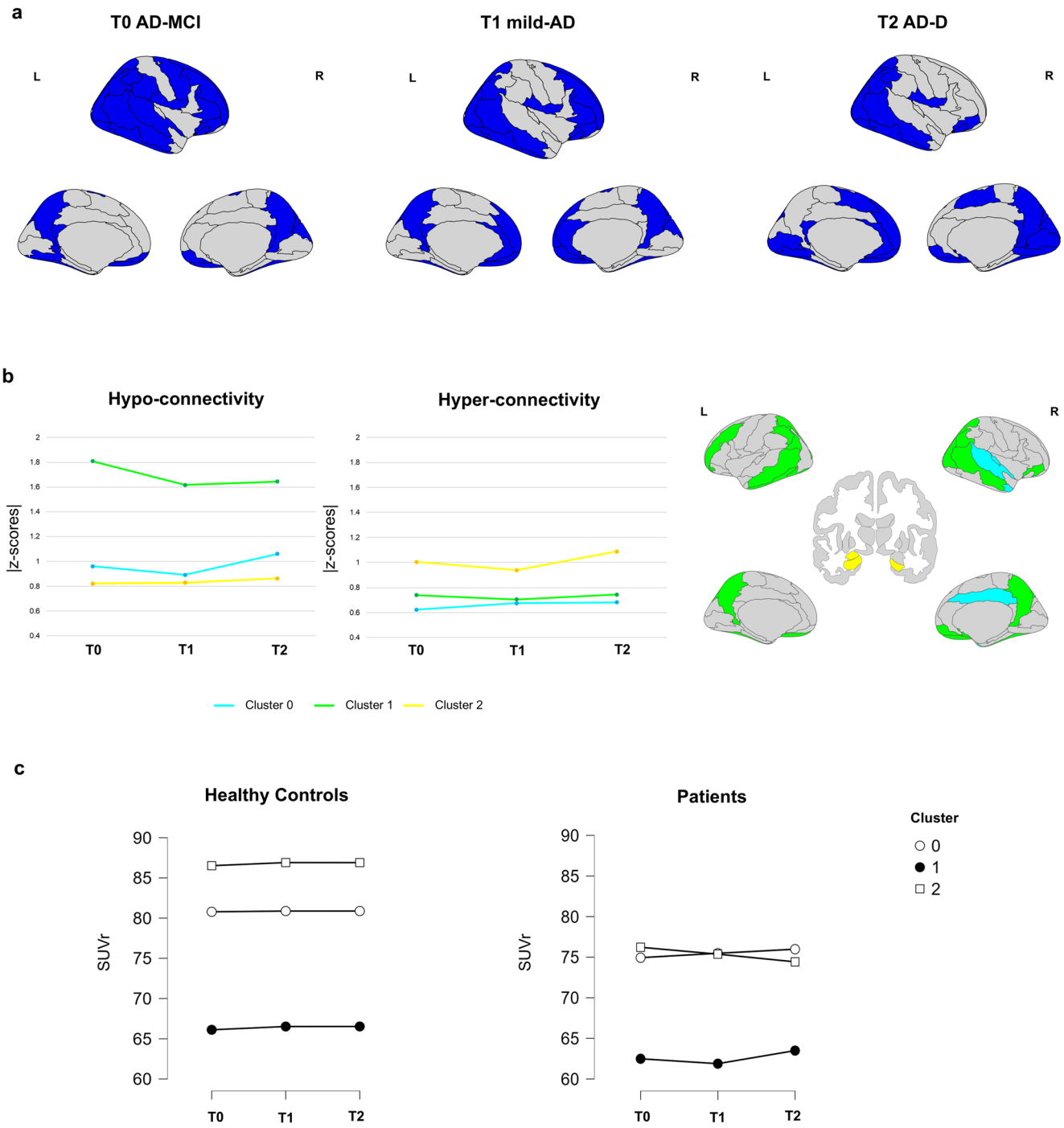

Fig. 2 Cluster analysis. (**a** – KLM1) Brain renderings depicting stage-specific altered nodes identified by KLM1. (**b** – KLM2) Line plots showing z-scores for each longitudinal cluster identified by KLM2, separated into hyper- and hypo-connectivity, respectively. Cluster 0 (cyan line) exhibited low values for both hypo- and hyper-connectivity, suggesting minimal differences between patients and healthy controls across stages. Cluster 1 (green line) showed greater negative z-scores, indicating consistent hypo-connectivity across stages. Cluster 2 (yellow line) exhibited greater positive z-scores, reflecting predominant hyper-connectivity. (**c**) Plots illustrating SUVr values at each time point within the longitudinal clusters identified by KLM2. Brain renderings were generated using the ggseg-suite packages developed by the Lifebrain EU project (https://www.lifebrain.uio.no/), led by the Center for Lifespan Changes in Brain and Cognition. *Abbreviations*: AD, Alzheimer's Disease; MCI, Mild Cognitive Impairment, AD-D, Dementia due to Alzheimer's Disease

Fig. 3 Spatial overlap analysis with Resting State Networks. Radar Plots showing spatial overlap between longitudinal Clusters and functional networks [31]. Box represents significant spatial overlap; dashed box represents a trend to significant overlap. **= $p < 0.01$; *= $p < 0.05$. Abbreviations: Visual, Visual Network; Default, Default Mode Network; DorsAttn, Dorsal Attentive Network; Control, Control Network; Sal/VenAttn, Salience/Ventral Attentive Network; Somatomotor, Somatomotor Network; Limbic, Limbic Network

Graph theory metrics

AD-MCI showed higher nodal degrees in limbic, parietal and cerebellar regions. Path length decreased in limbic and occipital areas; local efficiency declined in posterior regions; global efficiency increased in limbic and cerebellar areas; betweenness centrality decreased in temporal and occipital regions and clustering coefficients decreased in posterior regions and increased in limbic and cerebellar areas. More detailed results can be found in Supplementary material 5 and Supplementary Fig. 3.

Discussion

Previous cross-sectional studies with functional MRI showed inconsistent results about connectivity alterations in AD: some reported a decrease in functional connectivity within the DMN [35–37], while others suggested an increase [38–40]. These inconsistencies may reflect non-linear changes over time, with connectivity levels varying based on disease stage. Our study adopted a longitudinal approach across the whole brain of an AD cohort with positive markers for amyloid, tau, and neurodegeneration (A+/T+/N+), to reveal distinctive patterns of hypo- and hyper-connectivity alterations at three distinct clinical stages.

The transition from AD-MCI to full-blown dementia was marked by a spectrum of connectivity alterations, encompassing both hypo- and hyper-connectivity features. In particular, hyper-connectivity was detectable since the AD-MCI phases, predominantly in limbic and cerebellar regions. Hypo-connectivity instead, involved a widespread network of predominantly posterior cortical regions, since the AD-MCI phases.

Graph theory metrics highlighted AD associated decreasing connectivity efficiency in key posterior brain regions over time, except in limbic and cerebellar regions, notably the same regions which showed the most consistent hyper-connectivity.

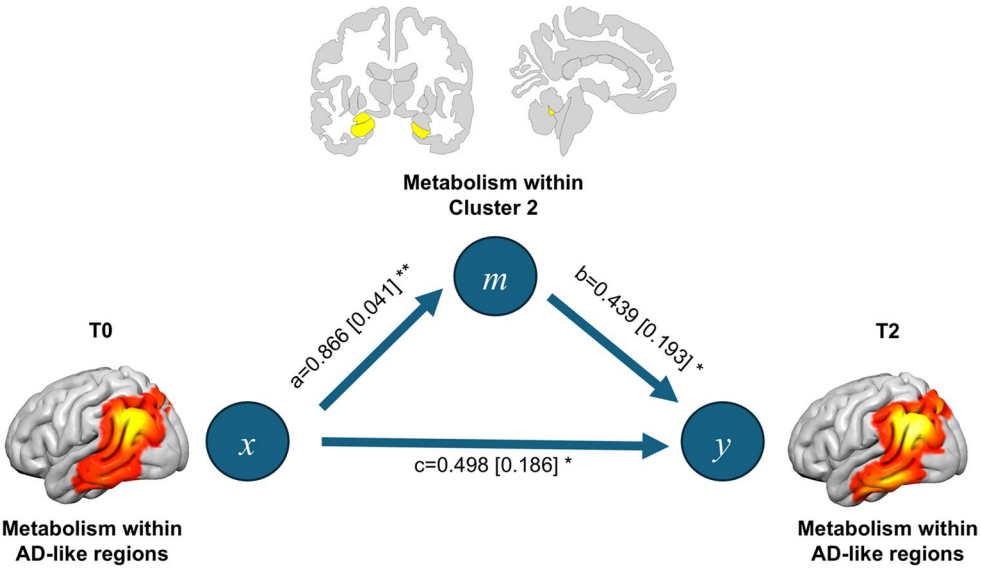

Fig. 4 Mediation analysis. Path diagram of the relationship between metabolism within AD-like parieto-temporal regions at T0 (AD-MCI) and T2 (AD-D) mediated by the metabolism within Cluster 2, assessed on the patients' sample. Path-weights are displayed as beta values with standard errors in brackets. Abbreviations: x, independent variable; y, dependent variable; m, mediator; AD, Alzheimer's Disease; β, standardized coefficient; *= $p < 0.05$; **= $p < 0.01$

Additionally, the assessment of connectivity reconfiguration at the whole-brain level, rather than focusing solely on specific resting state networks, allowed for the description of the interplay between the emerging connectivity patterns and the progression of brain hypometabolism at each stage. While regions consistently hypo-connected (Cluster 1) during the disease course were the same ones showing the most severe hypo-metabolism, the regions emerging in LC as constantly hyper-connected across the disease course (Cluster 2) were the ones showing the strongest longitudinal metabolic decrease, suggesting a different role of hypo- and hyper-connectivity in the neurodegenerative process. Of note, baseline metabolism in Cluster 2 was also identified as a significant mediator of AD-like parieto-temporal hypometabolism and a predictor of speed of conversion to dementia, highlighting its critical role in driving neurodegenerative changes in core AD regions and clinical progression over time.

In this study, we expand the previous evidence in four directions.

First, by using FDG-PET metabolic connectivity, we replicate the finding for presence of hyper-connectivity in AD, as it was measured via functional MRI (i.e., functional connectivity) [7, 14, 41–44]. While BOLD and FDG signals are both related to neural activity, via neurovascular and neurometabolic [45] coupling, respectively, they are not interchangeable, as shown by variably converging and diverging brain connectivity findings across the two modalities [46]. In particular, BOLD signal reflects the complex interplay between cerebral blood flow, blood volume, and metabolic rate of oxygen, as measured in the blood vessels [46]. FDG-PET reflects glucose metabolism, which is more directly coupled to excitatory neural activity based on glutamatergic transmission, as measured in astrocytes and neurons [46]. Our findings demonstrate that hyper-connectivity is detectable across different imaging modalities, such as FDG-PET, and not only limited to functional connectivity, as measured by means of BOLD signal of functional MRI.

Second, we showed that hyper-connectivity is not only present in the earliest disease phases [42, 43] but plays a role in the progression of disease phases. Our results in prodromal AD are in agreement with previous evidence [7, 42, 43], altogether indicating that hyper-connectivity is a very early phenomenon along the course of AD disease. The adoption of unsupervised clustering analysis allowed here the identification of groups of regions showing stage-specific alterations (STFC) and groups of regions showing consistent patterns of brain connectivity alterations along the disease course (LC).

Of note, we found a cluster of regions that were predominantly hyper-connected throughout the course of the disease. In particular, the medial temporal regions and vermis (LC Cluster 2) were characterized by greater hyper-connectivity than hypo-connectivity, consistently along the course of the disease. Increased connectivity in limbic regions has already been reported in AD patients [10, 12, 47] and appears to be a relevant mechanism in disease pathophysiology and clinical symptoms [12, 14]. Our results suggest that limbic network's nodes are more integrated in AD than HC, as indexed by increased degree, global efficiency and betweenness centrality, although the functional significance of this measure in pathology is far from clear. This might either: (1) reflect local compensatory mechanisms during early stages, in which increased connectivity in certain regions might counterbalance degeneration elsewhere, a phenomenon consistent with the Compensation-Related Utilization of Neural Circuits Hypothesis (CRUNCH; [48]). (2) reflect pathological mechanisms where Aβ pathology

would induce hyperactivity [49] and hyper-connectivity [7], as previously demonstrated for the medial temporal lobe. The limbic areas, specifically the medial temporal lobe, is considered an early site of tau pathology accumulation [50]. Notably, Hojjati et al. showed a mediation effect of hyper-connectivity on the association between cortical Aβ and early-phase limbic tau accumulation in AD [51]; the same mediation effect was replicated by Roemer-Cassiano et al. [7]. More recently, medial temporal hyperconnectivity was reported as a driver of hypometabolism and hippocampal atrophy [14].

Still, the bulk of the connectivity alterations predominantly involves regions of the default mode network (LC Cluster 1), showing predominant hypo-connectivity, consistently, throughout the course of the disease. These results are in accordance with previous evidence based on functional MRI showing that a predominant hypo-connectivity in DMN regions emerges as the disease progresses [41–44],.

Third, an in-depth analysis of hyper-connectivity showed that, hyper-connectivity was primarily driven by a switch in the direction of the correlation, observed in the MCI-AD and AD-D stage, from negative correlations, in controls, to positive correlations, in patients. This was particularly evident in the connections between cerebellar-limbic and cortical-cerebellar node connections. The present finding in HC is consistent with previous FDG-PET evidence showing strong negative correlations between cerebellum and cortical areas in healthy individuals [52]. While the nature of these negative correlations is unclear, one intriguing hypothesis is that, in healthy individuals, negative correlations might reflect a mechanism of efficient counter regulation of activity between the cortical and cerebellar network, where more limited energetic resources are allocated to the cerebellum to enhance cortical activity [52]. Based on our findings, it appears that this mechanism is lost in mild AD. Still, it must be noted that the biological interpretation of negative correlations remains debated, with some authors interpreting negative correlations as reflecting inhibition or deactivation [53], which suggest that methodological choices (e.g. global signal regression for fMRI, global mean scaling for PET) might be playing an important role in the emergence of artifactual negative correlations [54].

Fourth, and last, when investigating the relationship between hypo- and hyper-connectivity and glucose metabolism, as an index of (excitatory) synaptic dysfunction, we observed that regions consistently hyper-connected during the course of the disease were the only ones showing a significant and fast longitudinal decrease in glucose metabolism. In addition, the hyper-connected cluster was the only one showing a mediation effect on the AD-like parieto-temporal hypometabolism pattern progression. Further, glucose metabolism in the hyper-connected cluster, at baseline (MCI-AD) predicted the speed of conversion to dementia. We could speculate that an initial hyper-connectivity centered around the limbic circuit has a cascade of effects that may lead to severe neurodegeneration in the associative cortical areas in the advanced disease phase. Altogether, our findings suggest a negative role of hyper-connectivity in driving neurodegeneration, consistently with previous observations in other neurodegenerative diseases [38] and possibly against the hypothesis that hyper-connectivity might reflect compensatory mechanisms [19, 55, 56]. This is also consistent with the recent finding that hyper-connectivity drives tau pathology accumulation [7], and in keeping with the tight association between tau burden and neurodegeneration [57]. The interplay between Aβ and tau accelerates network dysfunction, while activated microglia near plaques amplify tau bioactivity through pro-inflammatory signaling and processing, creating a localized environment of increased connectivity that may precede synaptic collapse and neurodegeneration [58].

Our study has some limitations that warrant discussion. First, the HC and AD cohorts included in the current study significantly differed in terms of prevalence of APOE ε4 allele, however a finding in line with previous reports [59, 60]; while it is known that APOE ε4 alleles might affect glucose metabolism [61, 62] and brain connectivity [59], it is yet to be determined whether the APOE ε4 allele is specifically linked to hyper-connectivity. Unfortunately, the skewed distribution of the number of APOE ε4 alleles in our cohorts prevents us from investigating this aspect.

Second, we were unable to fully establish the prognostic value of hyper-connectivity-based markers. While we could prove that metabolism in hyper-connected regions predicts speed of conversion to dementia, we could not establish a linear relationship between metabolism in hyper-connected regions at baseline and cognitive chances, as assessed by ADNI-Mem scores. The limited sample size and homogeneity of our cohort may have reduced our ability to predict this cognitive outcome. Future studies involving larger and more heterogeneous samples will be essential to establish the predictive utility of early network alterations.

In addition, our original cohort selection—designed to ensure homogeneity and sufficient biomarker and clinical data across subjects—did not yield participants who met established criteria for preclinical AD. Future integration with the current dataset may extend our results to the full AD continuum.

In conclusion, brain hyper- and hypo-connectivity are observed throughout the AD longitudinal continuum; hyper-connectivity is present since the earliest pre-dementia phases (i.e. prior to conversion to AD dementia). The association of glucose metabolism in hyper-connected limbic regions with longitudinal decreases in temporoparietal glucose

metabolism and with the associated faster conversion to dementia, points to a pathological role of hyper-connectivity in driving neurodegenerative processes, rather than compensatory mechanisms. Overall, these results highlight a role of hyper-connectivity in AD disease neurodegeneration and disease progression, calling for further investigation of this understudied phenomenon.

Combining multimodal imaging techniques such as Amyloid-PET, Tau-PET, FDG-PET, and EEG could provide further insights into distinct connectivity clusters and underlying mechanisms. For instance, EEG could add a temporal dimension to connectivity analysis, revealing dynamic shifts in oscillatory networks and their interplay with structural and metabolic changes.

Supplementary Information The online version contains supplementary material available at https://doi.org/10.1007/s00259-025-07379-9.

Acknowledgements Data used in the preparation of this article were obtained from the Alzheimer's Disease Neuroimaging Initiative (ADNI) database (adni.loni.usc.edu). The investigators of the ADNI contributed to the design and implementation of the ADNI and/or provided data, but they did not participate in the analysis or writing of this report. A complete list of the ADNI investigators can be found at http://adni.loni.usc.edu/wpcontent/uploads/how_to_apply/ADNI_Acknowledgement_List.pdf.
CT has received personal fees for participating in advisory boards for Eli Lilly. APi has been supported by grants of Airalzh Foundation AGYR2021 Life-Bio Grant, The LIMPE-DISMOV Foundation Segala Grant 2021, the Italian Ministry of University and Research PRIN COCOON (2017MYJ5 TH) and PRIN 2021 RePlast (PRIN202039 WMFP), the H2020 IMI IDEA-FAST(ID853981), Italian Ministry of Health, Grant/Award Number: RF-2018-12366209 and PNRR-Health PNRR-MAD-2022-12376110. APa received grant support from the Italian Ministry of University and Research PRIN COCOON (2017MYJ5 TH) and PRIN 2021 RePlast (PRIN202039 WMFP), the H2020 IMI IDEA-FAST (ID853981), Italian Ministry of Health, Grant/Award Number: RF-2018-12366209, PNRR-Health PNRR-MAD-2022-12376110 and from CARIPLO Foundation.

Authors contribution A.G., R.M., M.I., A.S., and SP.C. performed the statistical analyses and interpretation of data for the work and drafted the manuscript. SP.C., A.G., L.P., A.S. contributed to the selection of patients and dataset preparation. A.G., R.M., M.I., A.S., SP.C., D.P., A.Pi., A.Pa., N.T, C.T. revised the manuscript. D.P., A.S., A.G., and SP.C. were responsible for the design and conceptualization of the study. D.P., A.S., A. Pi., A. Pa., C.T. and SP.C. contributed to data interpretation. All authors read and approved the final manuscript.

Funding Study supported by #NEXTGENERATIONEU (NGEU) funded by the Ministry of University and Research (MUR), National Recovery and Resilience Plan (NRRP), project MNESYS (PE0000006) – A multiscale integrated approach to the study of the nervous system in health and disease (DN. 1553 11.10.2022), by the Belgian National Fund for Scientific Research (grant number 40001328 to A.S., Chargée de Recherches F.R.S.-FNRS/Université de Liège/Coma Science Group GIGA).

Data availability All the data used in this study are publicly available in the ADNI repository (adni.loni.usc.edu).

Declarations

Ethics approval and consent to participate Written informed consent was obtained from participants. Data was used in the current study and the study was approved by all relevant ethic boards related to the ADNI project. The study was conducted in compliance with the Declaration of Helsinki for the protection of human participants.

Competing interests The authors declare no conflicts of interest.

Disclosure The authors report no disclosures relevant to the manuscript.

References

1. Jack CR, Bennett DA, Blennow K, et al. NIA-AA research framework: toward a biological definition of Alzheimer's disease. Alzheimer's Dement. 2018;14:535–62. https://doi.org/10.1016/j.jalz.2018.02.018.
2. Iaccarino L, Tammewar G, Ayakta N, et al. Local and distant relationships between amyloid, Tau and neurodegeneration in Alzheimer's disease. Neuroimage Clin. 2018;17:452–64. https://doi.org/10.1016/j.nicl.2017.09.016.
3. Pereira JB, Janelidze S, Ossenkoppele R, et al. Untangling the association of amyloid-β and Tau with synaptic and axonal loss in Alzheimer's disease. Brain. 2021;144:310–24. https://doi.org/10.1093/brain/awaa395.
4. Vogels T, Leuzy A, Cicognola C, et al. Propagation of Tau pathology: integrating insights from postmortem and in vivo studies. Biol Psychiatry. 2020;87:808–18. https://doi.org/10.1016/j.biopsych.2019.09.019.
5. Buckley RF, Schultz AP, Hedden T, et al. Functional network integrity presages cognitive decline in preclinical alzheimer disease. Neurology. 2017;89:29–37. https://doi.org/10.1212/WNL.0000000000004059.
6. Carli G, Tondo G, Boccalini C, Perani D. Brain molecular connectivity in neurodegenerative conditions. Brain Sci. 2021;11. https://doi.org/10.3390/brainsci11040433.
7. Roemer-Cassiano SN, Wagner F, Evangelista L, et al. Amyloid-associated hyperconnectivity drives Tau spread across connected brain regions in Alzheimer's disease. Sci Transl Med. 2025;17. https://doi.org/10.1126/scitranslmed.adp2564.
8. Berron D, van Westen D, Ossenkoppele R, et al. Medial Temporal lobe connectivity and its associations with cognition in early Alzheimer's disease. Brain. 2020;143:1233–48. https://doi.org/10.1093/brain/awaa068.
9. Das SR, Pluta J, Mancuso L, et al. Increased functional connectivity within medial Temporal lobe in mild cognitive impairment. Hippocampus. 2013;23:1–6. https://doi.org/10.1002/hipo.22051.
10. Pasquini L, Scherr M, Tahmasian M, et al. Link between hippocampus' Raised local and eased global intrinsic connectivity in AD. Alzheimer's Dement. 2015;11:475–84. https://doi.org/10.1016/j.jalz.2014.02.007.
11. Delli Pizzi S, Punzi M, Sensi SL. Functional signature of conversion of patients with mild cognitive impairment. Neurobiol Aging. 2019;74:21–37. https://doi.org/10.1016/j.neurobiolaging.2018.10.004.
12. Dautricourt S, de Flores R, Landeau B, et al. Longitudinal changes in hippocampal network connectivity in Alzheimer's disease. Ann Neurol. 2021;90:391–406. https://doi.org/10.1002/ana.26168.
13. Pasquini L, Rahmani F, Maleki-Balajoo S, et al. Medial Temporal lobe Disconnection and hyperexcitability across Alzheimer's

disease stages. J Alzheimers Dis Rep. 2019;3:103–12. https://doi.org/10.3233/ADR-190121.
14. Chauveau L, Landeau B, Dautricourt S et al. (2025) Anterior-temporal network hyperconnectivity is key to Alzheimer's disease: from ageing to dementia. Brain. https://doi.org/10.1093/brain/awaf008.
15. Jones DT, Knopman DS, Gunter JL, et al. Cascading network failure across the Alzheimer's disease spectrum. Brain. 2016;139:547–62. https://doi.org/10.1093/brain/awv338.
16. Rocchi F, Canella C, Noei S, et al. Increased fMRI connectivity upon chemogenetic Inhibition of the mouse prefrontal cortex. Nat Commun. 2022;13:1056. https://doi.org/10.1038/s41467-022-28591-3.
17. Crane PK, Carle A, Gibbons LE, et al. Development and assessment of a composite score for memory in the Alzheimer's disease neuroimaging initiative (ADNI). Brain Imaging Behav. 2012;6:502–16. https://doi.org/10.1007/s11682-012-9186-z.
18. Caminiti SP, Sala A, Presotto L, et al. Validation of FDG-PET datasets of normal controls for the extraction of SPM-based brain metabolism maps. Eur J Nucl Med Mol Imaging. 2021;48:2486–99. https://doi.org/10.1007/s00259-020-05175-1.
19. Agosta F, Pievani M, Geroldi C, et al. Resting state fMRI in Alzheimer's disease: beyond the default mode network. Neurobiol Aging. 2012;33:1564–78. https://doi.org/10.1016/j.neurobiolaging.2011.06.007.
20. Sala A, Lizarraga A, Caminiti SP, et al. Brain connectomics: time for a molecular imaging perspective? Trends Cogn Sci. 2023;27:353–66. https://doi.org/10.1016/j.tics.2022.11.015.
21. Aisen PS, Petersen RC, Donohue M, Weiner MW. Alzheimer's disease neuroimaging initiative 2 clinical core: progress and plans. Alzheimer's Dement. 2015;11:734–9. https://doi.org/10.1016/j.jalz.2015.05.005.
22. Della Rosa PA, Cerami C, Gallivanone F, et al. A standardized [18F]-FDG-PET template for Spatial normalization in statistical parametric mapping of dementia. Neuroinformatics. 2014;12:575–93. https://doi.org/10.1007/s12021-014-9235-4.
23. Perani D, Della Rosa PA, Cerami C, et al. Validation of an optimized SPM procedure for FDG-PET in dementia diagnosis in a clinical setting. Neuroimage Clin. 2014;6:445–54. https://doi.org/10.1016/j.nicl.2014.10.009.
24. Gallivanone F, Anthony Della Rosa P, Castiglioni I. Statistical Voxel-Based methods and [18F]FDG PET brain imaging: frontiers for the diagnosis of AD. Curr Alzheimer Res. 2016;13:682–94. https://doi.org/10.2174/1567205013666151116142039.
25. Perani D, Cerami C, Caminiti SP, et al. Cross-validation of biomarkers for the early differential diagnosis and prognosis of dementia in a clinical setting. Eur J Nucl Med Mol Imaging. 2016;43:499–508. https://doi.org/10.1007/s00259-015-3170-y.
26. Adamczuk K, De Weer A-S, Nelissen N, et al. Polymorphism of brain derived neurotrophic factor influences B amyloid load in cognitively intact Apolipoprotein E E4 carriers. Neuroimage Clin. 2013;2:512–20. https://doi.org/10.1016/j.nicl.2013.04.001.
27. Tzourio-Mazoyer N, Landeau B, Papathanassiou D, et al. Automated anatomical labeling of activations in SPM using a macroscopic anatomical parcellation of the MNI MRI Single-Subject brain. NeuroImage. 2002;15:273–89. https://doi.org/10.1006/nimg.2001.0978.
28. Laird NM, Ware JH. Random-Effects models for longitudinal data. Biometrics. 1982;38:963. https://doi.org/10.2307/2529876.
29. Titov D, Diehl-Schmid J, Shi K, et al. Metabolic connectivity for differential diagnosis of dementing disorders. J Cereb Blood Flow Metabolism. 2017;37:252–62. https://doi.org/10.1177/0271678X15622465.
30. Zhao H. Design and implementation of an improved K-Means clustering algorithm. Mob Inform Syst. 2022;2022:1–10. https://doi.org/10.1155/2022/6041484.
31. Sala A, Caprioglio C, Santangelo R, et al. Brain metabolic signatures across the Alzheimer's disease spectrum. Eur J Nucl Med Mol Imaging. 2020;47:256–69. https://doi.org/10.1007/s00259-019-04559-2.
32. Baron RM, Kenny DA. The moderator–mediator variable distinction in social psychological research: conceptual, strategic, and statistical considerations. J Pers Soc Psychol. 1986;51:1173–82. https://doi.org/10.1037/0022-3514.51.6.1173.
33. Thomas Yeo BT, Krienen FM, Sepulcre J, et al. The organization of the human cerebral cortex estimated by intrinsic functional connectivity. J Neurophysiol. 2011;106:1125–65. https://doi.org/10.1152/jn.00338.2011.
34. Mijalkov M, Kakaei E, Pereira JB, et al. BRAPH: A graph theory software for the analysis of brain connectivity. PLoS ONE. 2017;12:e0178798. https://doi.org/10.1371/journal.pone.0178798.
35. Wang Y, Risacher SL, West JD, et al. Altered default mode network connectivity in older adults with cognitive complaints and amnestic mild cognitive impairment. J Alzheimer's Disease. 2013;35:751–60. https://doi.org/10.3233/JAD-130080.
36. Zhou Y, Dougherty JH, Hubner KF, et al. Abnormal connectivity in the posterior cingulate and hippocampus in early Alzheimer's disease and mild cognitive impairment. Alzheimer's Dement. 2008;4:265–70. https://doi.org/10.1016/j.jalz.2008.04.006.
37. Zhu DC, Majumdar S, Korolev IO, et al. Alzheimer's disease and amnestic mild cognitive impairment weaken connections within the Default-Mode network: A Multi-Modal imaging study. J Alzheimer's Disease. 2013;34:969–84. https://doi.org/10.3233/JAD-121879.
38. Esposito R, Mosca A, Pieramico V, et al. Characterization of resting state activity in MCI individuals. PeerJ. 2013;1:e135. https://doi.org/10.7717/peerj.135.
39. Gardini S, Venneri A, Sambataro F, et al. Increased functional connectivity in the default mode network in mild cognitive impairment: A maladaptive compensatory mechanism associated with poor semantic memory performance. J Alzheimer's Disease. 2015;45:457–70. https://doi.org/10.3233/JAD-142547.
40. Zhang Z, Liu Y, Jiang T, et al. Altered spontaneous activity in Alzheimer's disease and mild cognitive impairment revealed by regional homogeneity. NeuroImage. 2012;59:1429–40. https://doi.org/10.1016/j.neuroimage.2011.08.049.
41. Sepulcre J, Sabuncu MR, Li Q, et al. Tau and amyloid B proteins distinctively associate to functional network changes in the aging brain. Alzheimer's Dement. 2017;13:1261–9. https://doi.org/10.1016/j.jalz.2017.02.011.
42. Schultz AP, Chhatwal JP, Hedden T, et al. Phases of hyperconnectivity and hypoconnectivity in the default mode and salience networks track with amyloid and Tau in clinically normal individuals. J Neurosci. 2017;37:4323–31. https://doi.org/10.1523/JNEUROSCI.3263-16.2017.
43. Fredericks CA, Sturm VE, Brown JA, et al. Early affective changes and increased connectivity in preclinical Alzheimer's disease. Alzheimer's Dementia: Diagnosis Assess Disease Monit. 2018;10:471–9. https://doi.org/10.1016/j.dadm.2018.06.002.
44. Guzmán-Vélez E, Diez I, Schoemaker D, et al. Amyloid-β and Tau pathologies relate to distinctive brain dysconnectomics in preclinical autosomal-dominant Alzheimer's disease. Proc Natl Acad Sci. 2022;119. https://doi.org/10.1073/pnas.2113641119.
45. Stoessl AJ. Glucose utilization: still in the synapse. Nat Neurosci. 2017;20:382–4. https://doi.org/10.1038/nn.4513.
46. Savio A, Fünger S, Tahmasian M, et al. Resting-State networks as simultaneously measured with functional MRI and PET. J Nucl Med. 2017;58:1314–7. https://doi.org/10.2967/jnumed.116.185835.
47. Gour N, Ranjeva J-P, Ceccaldi M, et al. Basal functional connectivity within the anterior Temporal network is associated

with performance on declarative memory tasks. NeuroImage. 2011;58:687–97. https://doi.org/10.1016/j.neuroimage.2011.05.090.
48. Reuter-Lorenz PA, Cappell KA. Neurocognitive aging and the compensation hypothesis. Curr Dir Psychol Sci. 2008;17:177–82. https://doi.org/10.1111/j.1467-8721.2008.00570.x.
49. Giorgio J, Adams JN, Maass A, et al. Amyloid induced hyperexcitability in default mode network drives medial Temporal hyperactivity and early Tau accumulation. Neuron. 2024;112:676–e6864. https://doi.org/10.1016/j.neuron.2023.11.014.
50. Lee WJ, Brown JA, Kim HR, et al. Regional Aβ-tau interactions promote onset and acceleration of Alzheimer's disease Tau spreading. Neuron. 2022;110:1932–e19435. https://doi.org/10.1016/j.neuron.2022.03.034.
51. Hojjati SH, Butler TA, de Leon M et al. (2024) Between-networks hyperconnectivity is induced by beta-amyloid and may facilitate tau spread.
52. Tomasi DG, Shokri-Kojori E, Volkow ND. Brain network dynamics adhere to a power law. Front Neurosci. 2017;11. https://doi.org/10.3389/fnins.2017.00072.
53. Sanchez-Catasus CA, Müller MLTM, De Deyn PP, et al. Use of nuclear medicine molecular neuroimaging to model brain molecular connectivity. PET and SPECT in neurology. Cham: Springer International Publishing; 2021. pp. 181–207.
54. Murphy K, Birn RM, Handwerker DA, et al. The impact of global signal regression on resting state correlations: are anti-correlated networks introduced? NeuroImage. 2009;44:893–905. https://doi.org/10.1016/j.neuroimage.2008.09.036.
55. Agosta F, Valsasina P, Absinta M, et al. Sensorimotor functional connectivity changes in amyotrophic lateral sclerosis. Cereb Cortex. 2011;21:2291–8. https://doi.org/10.1093/cercor/bhr002.
56. Gour N, Felician O, Didic M, et al. Functional connectivity changes differ in early and late-onset Alzheimer's disease. Hum Brain Mapp. 2014;35:2978–94. https://doi.org/10.1002/hbm.22379.
57. Boccalini C, Peretti DE, Mathoux G, et al. Early-phase 18F-Flortaucipir tau-PET as a proxy of brain metabolism in Alzheimer's disease: a comparison with 18F-FDG-PET and early-phase amyloid-PET. Eur J Nucl Med Mol Imaging. 2025. https://doi.org/10.1007/s00259-024-07063-4.
58. Palop JJ, Mucke L. Network abnormalities and interneuron dysfunction in alzheimer disease. Nat Rev Neurosci. 2016;17:777–92. https://doi.org/10.1038/nrn.2016.141.
59. Cacciaglia R, Operto G, Falcón C, et al. Genotypic effects of APOE-ε4 on resting-state connectivity in cognitively intact individuals support functional brain compensation. Cereb Cortex. 2023;33:2748–60. https://doi.org/10.1093/cercor/bhac239.
60. Mattsson N, Groot C, Jansen WJ, et al. Prevalence of the Apolipoprotein E E4 allele in amyloid B positive subjects across the spectrum of Alzheimer's disease. Alzheimer's Dement. 2018;14:913–24. https://doi.org/10.1016/j.jalz.2018.02.009.
61. Paranjpe MD, Chen X, Liu M, et al. The effect of ApoE E4 on longitudinal brain region-specific glucose metabolism in patients with mild cognitive impairment: a FDG-PET study. Neuroimage Clin. 2019;22:101795. https://doi.org/10.1016/j.nicl.2019.101795.
62. Knopman DS, Jack CR, Wiste HJ, et al. 18F-fluorodeoxyglucose positron emission tomography, aging, and Apolipoprotein E genotype in cognitively normal persons. Neurobiol Aging. 2014;35:2096–106. https://doi.org/10.1016/j.neurobiolaging.2014.03.006.